

14th CIRP Conference on Intelligent Computation in Manufacturing Engineering, CIRP ICME '20

On the Porous Structuring using Unit Cells

Yusuke Seto^a, AMM Sharif Ullah^{b,*}, Akihiko Kubo^b, Doriana Marilena D'Addona^c, Roberto Teti^c

^aGraduate School of Engineering, Kitami Institute of Technology, 165 Koen-Cho, Kitami 090-8507, Japan

^bDivision of Mechanical and Electrical Engineering, Kitami Institute of Technology, 165 Koen-Cho, Kitami 090-8507, Japan

^cDepartment of Chemical, Materials and Industrial, Production Engineering, University of Naples, Federico II Piazzale Tecchio 80, I – 80125, Naples, Italy

* Corresponding author. Tel.: +81-157-26-9207; fax: +81-157-26-9207. E-mail address: ullah@mail.kitami-it.ac.jp

Abstract

This study presents the characteristics of the eleven commonly used porous structures. The structures are designed using ten different unit cells. Some of the unit cells consist of free-form surfaces (e.g., triply periodic minimal surface). Some of them are straightforward in design (e.g., honeycomb structure). Some of them have a hybrid structure. The 3D CAD models of the structures are created using commercially available CAD software. The finite element analysis is conducted for each structure to know how it behaves under a static load. The structures are also manufactured using a 3D printer to confirm the manufacturability of them. It is found that some of the structures are easy to manufacture, and some are not. Particularly, metal-alloy-printed structures need a minimal thickness. However, the structures' printed or virtual models are evaluated by determining their respective mass, production cost, production time, Mises stress, and surface area. Using the values of mass, production time and cost, Mises stress, and surface area, the optimal structure is identified. Thus, the outcomes of this study can help identify the optimal porous structure for a given purpose.

© 2021 The Authors. Published by Elsevier B.V.

This is an open access article under the CC BY-NC-ND license (<https://creativecommons.org/licenses/by-nc-nd/4.0>)

Peer-review under responsibility of the scientific committee of the 14th CIRP Conference on Intelligent Computation in Manufacturing Engineering, 15-17 July 2020.

Keywords: porous structure; 3D printing; unit cell; scaffold; optimization

1. Introduction

The advent of 3D printing technology has created an excellent opportunity to fabricate complex structures using their digital models directly [1-7]. The basic steps of 3D printing technology are schematically illustrated in Fig. 1. This has brought challenges too. For example, one popular way to design complex structures is to use different types of scaffolds [8]. Unit cells are needed to design a scaffold.

A relatively comprehensive list of commonly used unit cells can be found in [8]. Some unit cells consist of free-form surfaces (e.g., triply periodic minimal surface [9]). Some of them are straightforward in design (e.g., honeycomb structure [10]). Some of them have a hybrid structure [8]. Each of them has a definite characteristic. Some of the structures are very heavy in terms of model data size. Some of the structure helps distribute loads, making them resilient against the load. Some

of them are very light. Some of them are costly. This way, several criteria can be used to characterize the structures.

Many authors have answered these questions, but in most cases, a very particular application is considered in the evaluation process. A general evaluation of the commonly used scaffold is not reported yet.

This article fills the abovementioned gap. In particular, this study presents the characteristics of the eleven commonly used porous structures.

The structures are designed using ten different unit cells. Some of the unit cells consist of free-form surfaces (e.g., triply periodic minimal surface). Some of them are straightforward in design (e.g., honeycomb structure). Some of them have a hybrid structure.

The 3D CAD models of the structures are created using commercially available CAD software.

The finite element analysis is conducted for each structure to know how it behaves under a static load. The structures are also manufactured using a 3D printer to confirm the manufacturability of them. The structures' printed or virtual models are evaluated by determining their respective mass, production cost, production time, Mises stress, and surface area. The results help determine the optimal structure is identified.

Thus, the article is organized as follows. Section 2 presents the unit cells and their CAD models. Section 3 presents the finite element analysis of the CAD models. Section 4 presents the 3D printed structures. Section 5 concludes this study.

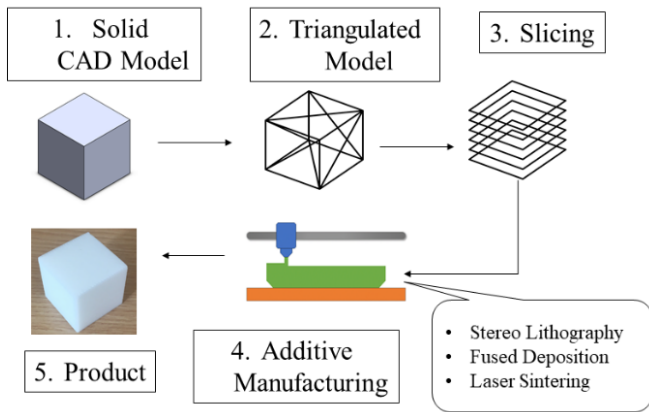


Fig. 1. 3D printing.

2. CAD Models

This section presents the CAD models of the porous structures. First, Table 1 summarizes the unit cells of the structures. The cells are numbered consecutively starting from 1 to 10. The cells denoted as 1, 2, and 5 are anisotropic unit cell [8]. The cells denoted as 3, 6, 9, and 10 are periodic uniform unit cells [8]. The cells denoted as 4, 7, and 8 are hybrid unit cells [8]. Each cell can be copied as many times as needed to create the corresponding porous structure.

The unit cells result in ten different porous structures, as summarized in Table 2.

The CAD models shown in Table 2 corresponding to the unit cells in Table 1, except model 11. Model 11 corresponds to a gradient model, which is created gradually increasing the pore size of unit cell 9. The load-bearing characteristics of the model can be determined using finite element analysis. This issue is described in Section 3.

However, the sizes (number of facets) of the triangulated models (see Fig. 1) are listed in Table 3. Among the CAD models shown in Table 3, the triangulated model of model 6 exhibits the minimal number of facets. The number is 3900. The number of facets of each model is divided by 3900 to calculate how many times the triangulated model is larger than model 6.

The results are shown in the rightmost column in Table 3. The results indicate that if free-formed surfaces are used, the model's size increases many folds than the non-free-formed model.

The surface area versus the mass of the models is shown in Fig. 2. As seen in Fig. 2, models 1, 2, 3, 6, and 8 have very low mass. Among these models, model 8 has the highest surface area, and model 6 has the lowest area. Model 2, 5, 9, and 8 has almost the same surface area. When surface area and mass are considered together, model 6 is the lightest, and model 8 is the most surface-contained.

Table 1. Unit cells of the porous structures.

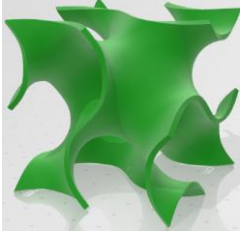
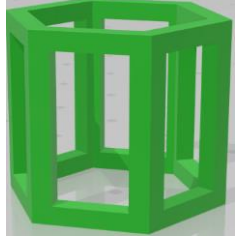
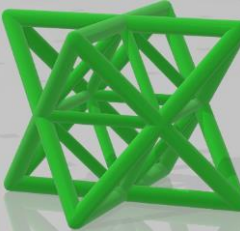


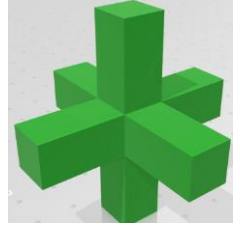
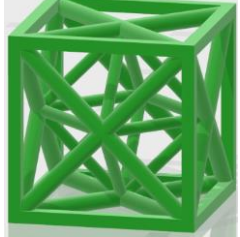
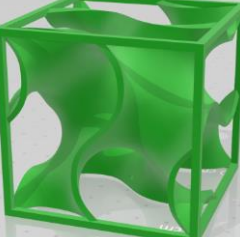


	
①	②
	
③	④
	
⑤	⑥
	
⑦	⑧
	
⑨	⑩

Table 2. CAD models of the porous structures.

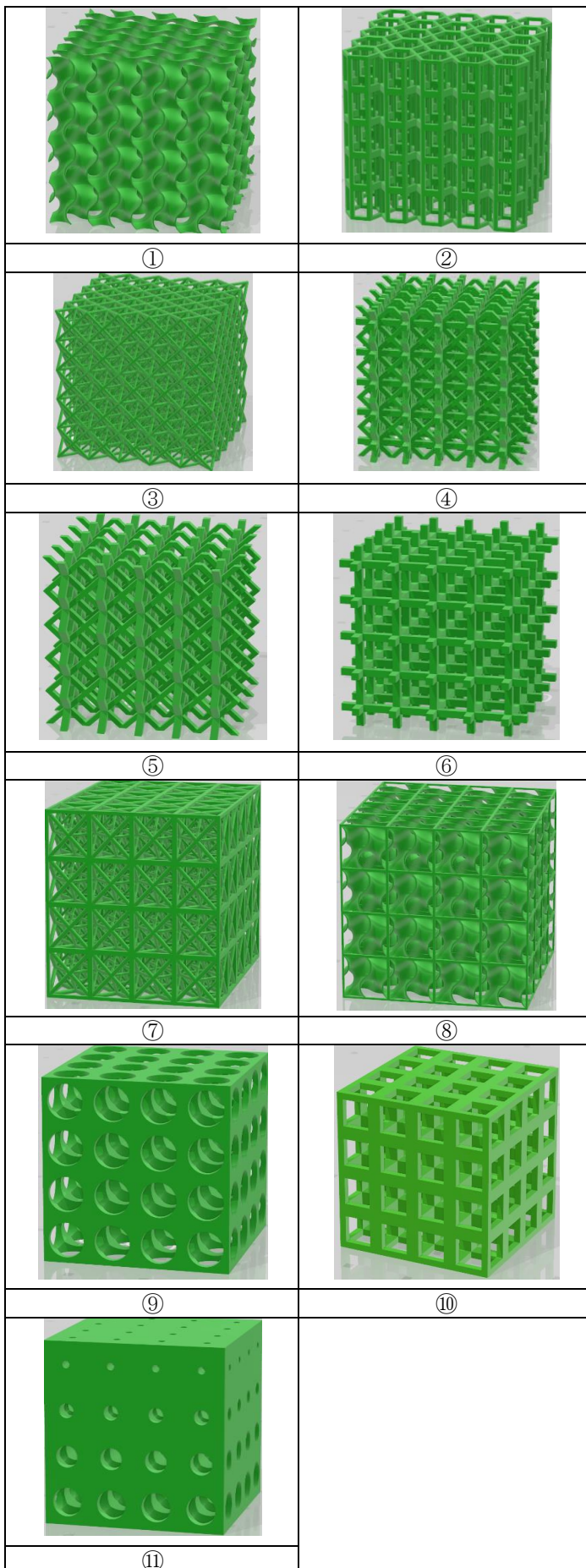


Table 3. Sizes of the models.

CAD Model	Facets	Times (about)
1	1570616	402.72
2	17400	4.46
3	727850	186.63
4	16900	4.33
5	10040	2.57
6	3900	1
7	546248	140.06
8	1668716	427.88
9	59712	15.31
10	4940	1.27
11	69420	17.8

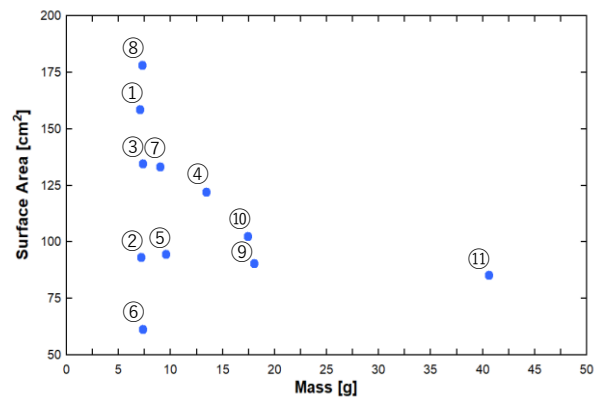


Fig. 2. Surface area versus mass of the models.

3. Load-Bearing Capacity

The load-bearing capacity of each model in Table 2 is determined using finite element analysis. The load-distribution of each model is shown in Table 4. In this analysis, the following settings are used. The load is a static load equal to 100 N. The material used is pure Titanium where the density is equal to $4.53 \cdot 10^{-3}$ g/mm³, tensile strength is equal to 344.5 MPa, modulus of elasticity is equal to 102.8 GPa, and the Poisson ratio is equal to 0.361.

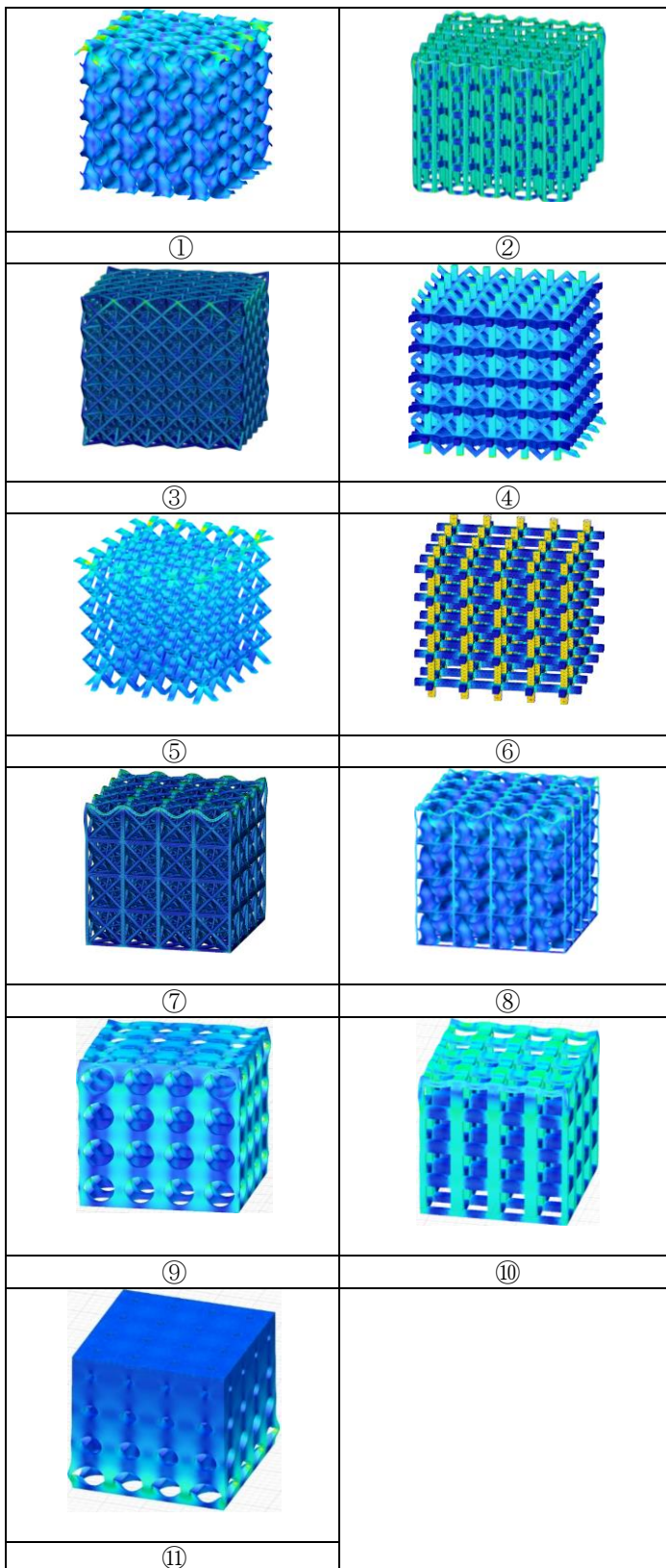
As far as the mesh size is concerned, 4% of the average size of a facet is used to set the mesh size. This means that the mesh size is very small for free-form surface-based models, whereas, for straightforward models, the mesh size is relatively large.

As seen in Table 4, graduation in color represents the stress distribution. The colors close to blue represent low-stress regions, whereas the colors close to yellow represent high-stress regions.

Based on the model, the stress distribution exhibits a different kind of characteristics. For example, in model 1, the upper region of the model exhibits high stress, whereas the lower region exhibits a systematic variation in the stress distribution.

A different scenario is seen in the case of model 6. In this case, the region parallel to the load exhibits high-stress concentration, whereas the region perpendicular to the load exhibit low-stress concentration.

Table 4. Load-bearing capability of the structures



The remarkable thing is that for model 2 (honeycomb structure), the stress distribution is not as severe as other models. This means that it might exhibit low von Mises stress [11-17] compared to other models.

Therefore, von Mises stress is calculated for each model. The results are shown in Fig. 3. As seen in Fig. 3, model 2 is

the best one compared to others in terms of von Mises stress and mass. Models 9, 10, and 11 perform similar to model 2 in terms of load-bearing capacity, but their mass is high, and model 11 has the highest mass. This means that model 2, 9, 10, and 11 are the best for load-bearing capacity. Models 1, 3, ..., 8 are not suitable from the viewpoint of load-bearing capacity though they are not heavy. Model 8 exhibits the highest stress concentration. It is a hybrid model where the outer boundary exhibits a straightforward geometry, but it consists of free-form surfaces. This means that it is not good to create a hybrid structure using a straightforward and free-form surface.

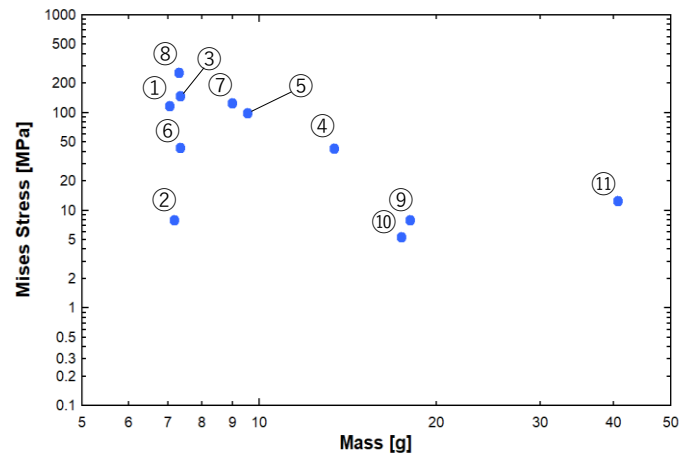


Fig. 3. von Mises stress versus Mass of the models.

4. 3D Printed Structures

This section shows some of the 3D printed structures. The goal is to outline the manufacturability of the structures. An ordinary 3D printer is used to fabricate the structure shown in Table 5. The printing conditions are as follows: PLA filament, 100% filling rate, the 0.1 mm layer thickness.

The printed structures 1, ..., 6 correspond to models 1, ..., 6, respectively. The other printed structure (structure 7) corresponds to model 10. The edges of structure 1 is not fabricated accurately. Structure 2 is a small-scaled structure of model 2. Some of the openings are filled by material creating inaccuracy due to this small-sizing. Whereas the inner segment is fabricated without any inaccuracy. This means that the outer region is subjected to fabrication inaccuracy due to scaling or free-formedness. If the unit cells' connections (struts) are made thick enough, then the fabrication accuracy increases. This is confirmed by the fabricated structures 3, ..., 7, as shown in Table 5.

However, the production time (time needed to print the structures) and the cost (cost is calculated by the cost of material consumed) are shown in Fig. 4. There is a strong correlation between production time and cost. Based on these two criteria, model 6 is the best, and model 11 spends the most time and cost. The others are between these two extremes.

The remarkable thing is that both the free-formed surface and straightforward geometry-based structure can be made without consuming more time and cost. In this respect, the production time and cost of models 1, 5, and 6 can be compared.

Table 5. Some 3D printed structures.

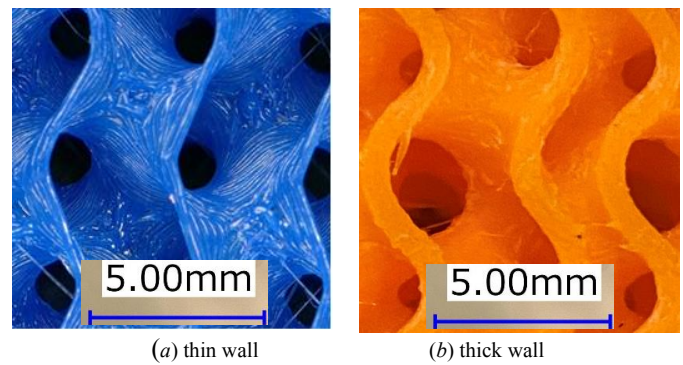
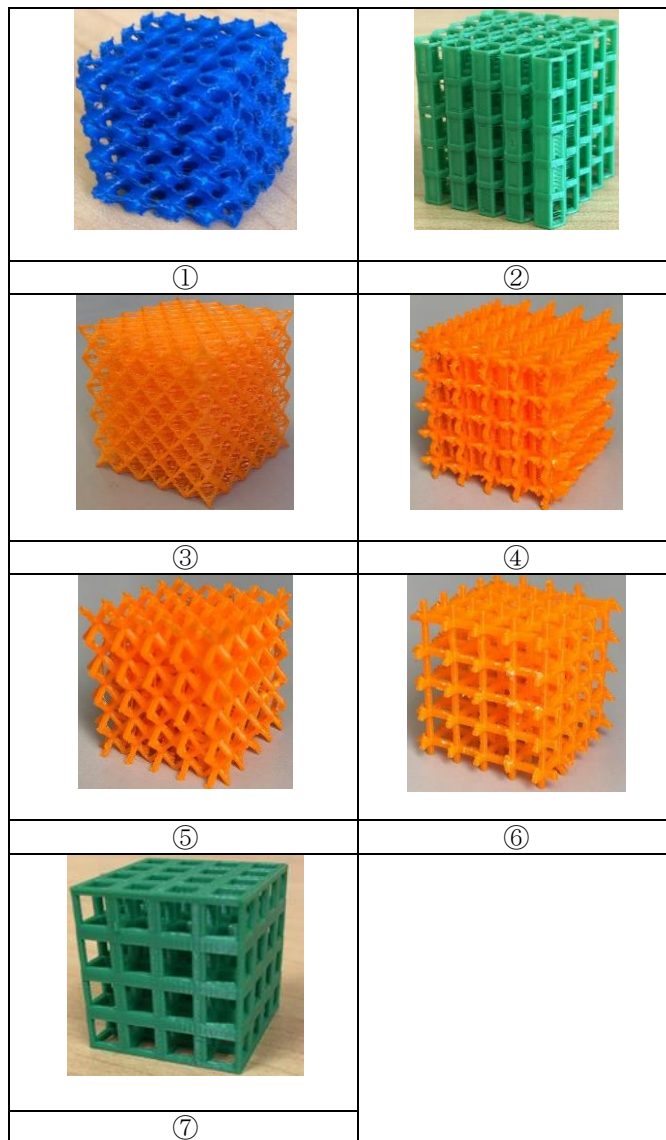


Fig. 5. Effect of strut and wall thickness.

The same model is manufactured using different wall thicknesses. Fig. 5 shows the picture of one of the structures printed in two different walls (strut) thicknesses. This picture reveals that even if the filling rate is kept the same during the fabrication process, the printed structure may not be accurate due to a thin wall. This tendency becomes stronger, especially when the layers are not vertically stacked in the free-form surface-based model.

In addition, the thin-walled structure (Fig. 5(a)) exhibits a rough surface in the connecting areas of the unit cells. This is not the case for the thick-walled structure (Fig. 5(b)). This means that if free-form surface-based unit cells are used to fabricate a porous structure; the wall thickness must be kept as thick as possible.

If the thickness cannot be increase, the pitch of the printing layer thickness can be reduced. This measure increases the number of layers in the fabrication process, resulting in a longer printing time. The same argument is true for the metallic printing process.

One of the examples is shown in Fig. 6. It is free-form surface-based structure, which underlies model 1. In this case, pure Titanium is used to fabricate the structure. The wall and strut thickness is 1 mm.

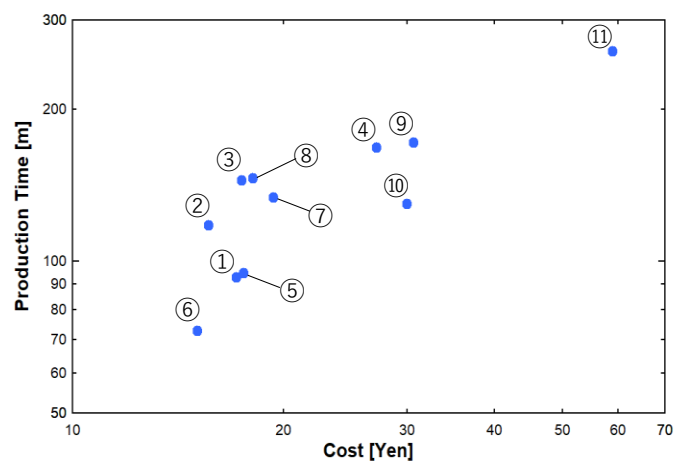


Fig. 4. Production time versus cost of the structures.



Fig. 6. Metallic porous structure.

5. Concluding Remarks

The unit cell-based geometric modeling can easily create a shape with a complicated internal structure. This approach is particularly effective in maintaining the regularity of an internal structure.

Besides, the unit cell can be modified easily, making them more additive manufacturing friendly, e.g., the strut and wall thickness of the unit cell, and thereby, the model can be modified without any extract modeling effort to ensure 3D printing constraint.

As far as a porous structure's load-bearing capacity is concerned, a honeycomb-like simple structure is recommended; hybrid unit cells combining free-form surface and straightforward geometry may not be good.

Models made of orthogonal struts likely to consume less printing materials and time. If pores are not adjusted using a gradient function (for example, model 11) significantly changes its characteristics in load-bearing capacity, surface area, cost, and fabrication time.

Wall thickness of the model and layer thickness of the printing process are critical parameters to ensure the accuracy of the 3D printed unit-cell based porous structure.

The outcomes of this study can find out the optimal structure for a given purpose.

References

- [1] Van der Geer J, Hanraads JAJ, Lupton RA. The art of writing a scientific article. *J Sci Commun* 2000; 163: 51-9.
- [2] Ferretti S, Caputo D, Penza M, D'Addona DM. Monitoring Systems for Zero Defect Manufacturing. *Procedia CIRP* 2013; 12: 258-263.
- [3] Mekid S, Schlegel T, Aspragathos N, Teti R. Foresight formulation in innovative production, automation and control systems. *Foresight* 2008; 9(5): 35–47.
- [4] Bourell DL, Rosen DW, Leu MC. The Roadmap for Additive Manufacturing and Its Impact. *3D Printing and Additive Manufacturing* 2014; 1 (1): 6-9.
- [5] Gibson I, Rosen D, Stucker B. *Additive Manufacturing Technologies: 3D Printing, Rapid Prototyping, and Direct Digital Manufacturing*. Springer, New York, NY, 2015.
- [6] Ullah AMMS, Kiuno H, Kubo A, D'Addona DM. A system for designing and 3D printing of porous structures. *CIRP Annals* 2020; 69/1: 113-116.
- [7] Ullah AMMS, D'Addona DM, Harib K, Lin T. Fractals and Additive Manufacturing. *Int. J. Automation Technol.* 2016; 10 (2): 222-230.
- [8] Strunk Jr W, White EB. *The elements of style*. 3rd Ed. New York, Macmillan, 1979.
- [9] Gibson I, Rosen D, Stucker B. *Additive Manufacturing Technologies: 3D Printing, Rapid Prototyping, and Direct Digital Manufacturing*. Springer, New York, NY, 2015.
- [10] Zhang X, Fang G, Zhou J. Additively Manufactured Scaffolds for Bone Tissue Engineering and the Prediction of their Mechanical Behavior. *Materials* 2017, 10 (1): 50.
- [11] Ozbolat I, Gudapati H. A Review on Design for Bioprinting. *Bioprinting* 2016, 3-4: 1-14.
- [12] Ullah AMMS. Design for Additive Manufacturing of Porous Structures Using Stochastic Point-Cloud. *Computer-Aided Design and Applications* 2018, 15 (1): 138-146.
- [13] Ghouse S, Babu S, Nai K, Hooper PA, Jeffers JRT. The Influence of Laser Parameters, Scanning Strategies and Material on the Fatigue Strength of a Stochastic Porous Structure. *Additive Manufacturing* 2018, 22: 290-301.
- [14] Wang S, Shi Z, Liu L, Zhou X, Zhu L, Hao Y. The design of Ti6Al4V Primitive surface structure with symmetrical gradient of pore size in biomimetic bone scaffold. *Materials & Design* 2020; 193.
- [15] Maskery I, Sturm L, Aremu AO, Panesar A, Williams CB, Tuck CJ, Wildman RD, Ashcroft IA, Hague RJM. Insights into the mechanical properties of several triply periodic minimal surface lattice structures made by polymer additive manufacturing. *Polymer* 2018; 152: 62-71.
- [16] Huan Z, Chu HK, Yang J, Sun D. Characterization of a Honeycomb-Like Scaffold With Dielectrophoresis-Based Patterning for Tissue Engineering. *IEEE Trans Biomed Eng* 2017; 64(4): 755-764.
- [17] Wang H, Liu J, Wen G, Xie YM. The robust fail-safe topological designs based on the von Mises stress- Finite Elements in Analysis and Design 2020; 171: 103376.